


ONCOLOGY



Intraindividual comparison of CT and MRI for predicting vessels encapsulating tumor clusters in hepatocellular carcinoma

Junhan Pan¹, Huizhen Huang¹, Siying Zhang¹, Yanyan Zhu¹, Yuhao Zhang², Meng Wang², Cong Zhang¹, Yan-Ci Zhao¹ and Feng Chen^{1*} 

Abstract

Objectives To establish and validate scoring models for predicting vessels encapsulating tumor clusters (VETC) in hepatocellular carcinoma (HCC) using computed tomography (CT) and magnetic resonance imaging (MRI), and to intra-individually compare the predictive performance between the two modalities.

Methods We retrospectively included 324 patients with surgically confirmed HCC who underwent preoperative dynamic CT and MRI with extracellular contrast agent between June 2019 and August 2020. These patients were then divided into a discovery cohort ($n = 227$) and a validation cohort ($n = 97$). Imaging features and Liver Imaging Reporting and Data System (LI-RADS) categories of VETC-positive HCCs were evaluated. Logistic regression analyses were conducted on the discovery cohort to identify clinical and imaging predictors associated with VETC-positive cases. Subsequently, separate CT-based and MRI-based scoring models were developed, and their diagnostic performance was compared using generalized estimating equations.

Results On both CT and MRI, VETC-positive HCCs exhibited a higher frequency of size > 5.0 cm, necrosis or severe ischemia, non-smooth tumor margin, targetoid appearance, intratumor artery, and heterogeneous enhancement with septations or irregular ring-like structure compared to VETC-negative HCCs (all $p < 0.05$). Regarding LI-RADS categories, VETC-positive HCCs were more frequently categorized as LR-M than VETC-negative cases (all $p < 0.05$). In the validation cohort, the CT-based model showed similar sensitivity (76.7% vs. 86.7%, $p = 0.375$), specificity (83.6% vs. 74.6%, $p = 0.180$), and area under the curve value (0.80 vs. 0.81, $p = 0.910$) to the MRI-based model in predicting VETC-positive HCCs.

Conclusion Preoperative CT and MRI demonstrated comparable performance in the identification of VETC-positive HCCs, thus displaying promising predictive capabilities.

Clinical relevance statement Both computed tomography and magnetic resonance imaging demonstrated promise in preoperatively identifying the vessel-encapsulating tumor cluster pattern in hepatocellular carcinoma, with no statistically significant difference between the two modalities, potentially adding additional prognostic value.

Junhan Pan and Huizhen Huang contributed equally to this work.

*Correspondence:

Feng Chen

chenfenghz@zju.edu.cn

¹Department of Radiology, The First Affiliated Hospital of Zhejiang University School of Medicine, No.79 Qingchun Road, Hangzhou 310003, China

²Department of Pathology, The First Affiliated Hospital of Zhejiang University School of Medicine, No.79 Qingchun Road, Hangzhou 310003, China

Key Points

- *Computed tomography (CT) and magnetic resonance imaging (MRI) show promise in the preoperative identification of vessels encapsulating tumor clusters-positive hepatocellular carcinoma (HCC).*
- *HCC with vessels encapsulating tumor cluster patterns were more frequently LR-M compared to those without.*
- *These CT and MRI models showed comparable ability in identifying vessels encapsulating tumor clusters-positive HCC.*

Keywords Hepatocellular carcinoma, Diagnosis, Computed tomography, Magnetic resonance imaging, Metastasis

Introduction

Vessels encapsulating tumor clusters (VETC), a distinct histological vascular pattern, is closely associated with a mechanism of metastasis in hepatocellular carcinoma (HCC) [1]. The VETC pattern is characterized by sinusoid-like vessels encapsulating individual tumor clusters and forming unique cobweb-like patterns [1, 2]. Patients with VETC-positive HCCs typically exhibit greater tumor burden, elevated alpha-fetoprotein (AFP) levels, and worse prognosis compared to those with VETC-negative HCC [1, 3]. As a robust prognostic biomarker, VETC can also offer guidance for treatment strategies in patients undergoing liver transplantation, surgical resection, and systemic therapies [4–7]. Thus, identification of VETC-positive HCCs before initiating treatments may have important implications for tailoring therapies and predicting prognosis. However, the assessment of VETC relies on the biological specimen, which introduces potential sampling errors and requires post-operative evaluation.

Unlike other malignancies, the diagnosis of HCC in high-risk individuals can be achieved through stringent imaging criteria without invasive procedures [8, 9]. Multiphase computed tomography (CT) and multiparametric magnetic resonance imaging (MRI) are commonly employed for HCC diagnosis, each with its own strengths and weaknesses [10]. While MRI provides enhanced soft tissue contrast and avoids radiation exposure, practical considerations like cost, scan time, and patient contraindications may limit its utility. In such situations, CT may serve as a more suitable option. Beyond the imaging diagnosis, accumulating evidence suggests that imaging features may provide valuable insights into the biological aggressiveness of HCC [11]. Recent studies also demonstrated a significant correlation between several CT and MRI characteristics and the presence of VETC patterns in HCC [7, 12–16]. Furthermore, diagnostic models integrating these conventional imaging features have shown promising performance, with area under the curve (AUC) values ranging from 0.69 to 0.84 on CT [7, 12] and 0.59 to 0.89 on MRI [14, 16]. Given the practical significance of imaging in predicting VETC, it is crucial to comprehensively understand the capabilities and strengths of both CT and MRI modalities.

The Liver Imaging Reporting and Data System (LI-RADS) provides a standardized framework for characterizing liver findings in individuals at risk of HCC [8]. In addition to the hepatic lesion characterization, recent studies have revealed the prognostic significance of LI-RADS categories. Specifically, HCCs classified as LR-M exhibit more aggressive tumor biology compared to those categorized as LR-4/5 [17–19]. However, few studies have comprehensively explored the distributions of LI-RADS categories in VETC-positive and VETC-negative HCCs on both CT and MRI modalities.

Therefore, this study aimed to systemically elucidate the imaging features and LI-RADS categories associated with VETC-positive HCCs at dynamic CT and extracellular contrast agent-enhanced MRI. Furthermore, we will develop and validate a separate scoring model based on CT and MRI for identifying VETC-positive HCCs and conduct a head-to-head comparison of their predictive abilities.

Materials and methods**Study population**

This retrospective study received ethical approval from the local Institutional Review Board (approval number: IIT20220893A) and the requirement for written informed consent was waived. Between June 2019 and August 2020, consecutive patients who underwent surgical resection for HCC at our institution were included in this study. Inclusion criteria were: (a) pathologically confirmed HCC, (b) receiving both dynamic CT and extracellular contrast agent-enhanced MRI within 1 month before surgery, (c) available clinical laboratory data and pathology slides, (d) without any HCC treatments prior to surgery. Exclusion criteria were: (a) having any prior or current malignancy other than HCC, (b) incomplete image data or inadequate image quality, or (c) having macrovascular invasion or extrahepatic metastasis. All images were retrieved from a picture archiving and communication system and evaluated by a radiologist with 5 years of expertise in liver imaging, who was not involved in the further imaging analysis. Detailed criteria for assessing image data completeness and quality can be found in Tables S1 and S2. The eligible patients were randomly divided into a

discovery cohort and a validation cohort in a 7:3 ratio using computer-generated randomization. Patient demographics, liver disease etiology, Child-Pugh class, albumin-bilirubin grade, serum AFP, and aspartate aminotransferase were extracted from electronic medical records.

Imaging technique

Dynamic CT and extracellular contrast agent-enhanced MRI examinations were performed using 256-row systems and 3.0-T systems, respectively. The dynamic CT examination included precontrast, arterial phase, portal venous phase, and delayed phase images. Arterial phase scanning began approximately 20 s after the descending aorta reached an enhancement of 100 HU, as measured using a bolus-tracking technique. Portal venous and delayed phase images were acquired at 60–75 s and 150–180 s, respectively, after contrast agent injection. The MRI protocol included fat-suppressed T2-weighted, in- and opposite-phase T1-weighted, contrast-enhanced T1-weighted, and diffusion-weighted imaging with corresponding apparent diffusion coefficient maps. The arterial phase, portal venous phase, and delayed phase images were obtained at 14–20 s, 45–60 s, and 150–180 s, respectively, following contrast agent injection. Detailed descriptions of the CT and MRI protocols can be found in Appendix E1.

Histopathological examination

All histopathological slides were examined by a pathologist (with 12 years of experience in liver pathology) who was blinded to the clinical and imaging data. For cases with multiple lesions, the largest lesion was selected as the target for both pathology and imaging analyses. The study recorded pathological factors, including tumor size, Edmondson grade, presence of satellite nodules, microvascular invasion, and the VETC pattern. The VETC pattern was determined by assessing the CD34 immunostaining. HCC sections showing a VETC pattern were classified as VETC-positive, while those without any VETC pattern were classified as VETC-negative [1, 4, 12].

Imaging analysis

Two radiologists with 6 and 10 years of experience in liver imaging respectively, independently assessed the presence of the imaging features, while being blinded to the clinical data and final diagnosis. The initial analysis focused on CT scans, followed by a subsequent review of MRI scans after a one-month interval [20]. All cases were presented in a randomized order for each reader's evaluation of both CT and MRI. In case of disagreements between the two radiologists, consensus was achieved through discussions. Features a-o were evaluated on both CT and MRI, while

features p-s were solely analyzed on MRI: (a) size > 5.0 cm, (b) non-rim arterial phase hyperenhancement (APHE), (c) non-peripheral washout, (d) enhancing "capsule", (e) corona enhancement, (f) mosaic architecture, (g) fat in mass more than adjacent liver, (h) blood products in mass, (i) rim APHE, (j) delayed central enhancement, (k) necrosis or severe ischemia, (l) intratumor artery, (m) non-smooth tumor margin, (n) incomplete "capsule", (o) types of enhancement pattern (type-1, homogeneous hypoenhancement without increased arterial blood flow; type-2, homogeneous hyperenhancement with increased arterial blood flow; type-3, heterogeneous enhancement with septations; and type-4, heterogeneous enhancement with irregular ring-like structures) [7, 15, 21], (p) mild-moderate T2 hyperintensity, (q) restricted diffusion, (r) targetoid restriction, and (s) marked diffusion restriction. All definitions of imaging features are presented in Table S3. Afterward, LI-RADS categorization was performed for patients at high risk for HCC, including those with cirrhosis, chronic hepatitis B viral infection, and current or prior HCC [8].

Quantitative analyses on the arterial phase, portal venous phase, and apparent diffusion coefficient images were further performed by another radiologist with 5 years of experience in liver imaging. Circular regions of interest were positioned on transverse slices at the maximal diameter of the tumor while excluding peripheral portions to minimize potential partial volume effects [13]. Furthermore, regions of interest measuring 200–300 mm² were positioned on normal liver parenchyma, avoiding major vasculature and artifacts [22]. The measurements of the tumor and adjacent liver parenchyma for each case were repeated three times, and the average values were used for subsequent analysis. The ratios of tumor-to-liver attenuation or signal intensity were calculated on arterial phase and portal venous phase images from both CT and MRI scans. Similarly, the ratio of tumor-to-liver parametric values was computed on the respective apparent diffusion coefficient maps from MRI scans [22].

Construction of the scoring models

Continuous variables were transformed into binary variables based on either normal laboratory ranges or receiver operating characteristic (ROC) curve analysis. The maximum number of variables for multivariable logistic regression analysis was determined based on 20% of VETC-positive cases in the discovery cohort [23]. Univariable and multivariable logistic regression analyses were performed using a backward stepwise approach to identify clinical and imaging predictors of VETC-positive HCCs. The optimal combination of predictors was determined through five-fold cross-validation and the Akaike Information Criterion. Separate scoring models

for CT and MRI were developed by integrating significant predictors and assigning weights based on their regression coefficients. ROC analysis with the Youden index was used to determine the optimal threshold for each scoring model.

Statistical analysis

Continuous variables were compared by ANOVA or Mann–Whitney *U*-test and categorical variables were analyzed by chi-squared or Fisher's exact test. Kappa coefficients were utilized to evaluate inter-reader and inter-modality agreement and were classified as follows: 0.00–0.20, slight agreement; 0.21–0.40, fair; 0.41–0.60, moderate; 0.61–0.80, substantial; and 0.81–1.00, almost perfect. The sensitivity, specificity, negative predictive value, and positive predictive value of the CT-based model and the MRI-based scoring models were calculated to evaluate their diagnostic performance. The diagnostic performance of the models was evaluated through ROC analysis and calibration curve analysis. Generalized estimating equations were utilized to compare the sensitivity, specificity, and AUCs between the models. Subgroup analysis was conducted for HCC cases with surgical

tumor size ≤ 5.0 cm and ≤ 3.0 cm. All statistical analyses were performed in R software (version 4.3.1; The R Foundation for Statistical Computing, Vienna, Austria). Two-sided $p \leq 0.05$ was considered to indicate significance.

Results

Clinical and pathological characteristics

A total of 324 patients (262 male; median age, 59 years \pm 11) were included in this study, with 227 in the discovery cohort and 97 in the validation cohort (Fig. 1). There were no statistically significant differences in clinical and pathological characteristics between the two cohorts (all $p > 0.05$) (Table 1). Sixty-nine (30.4%) and 30 (30.9%) HCCs were categorized as VETC-positive cases in the discovery and validation cohort, respectively. One-hundred sixty-one HCCs (70.9%) in the discovery cohort and 70 HCCs (72.2%) in the validation cohort had a surgical tumor size ≤ 5.0 cm. Patients with VETC-positive HCC had significantly higher serum AFP, larger surgical tumor size, and a higher incidence of microvascular invasion compared to those with VETC-negative cases (all $p \leq 0.05$) (Table S4).

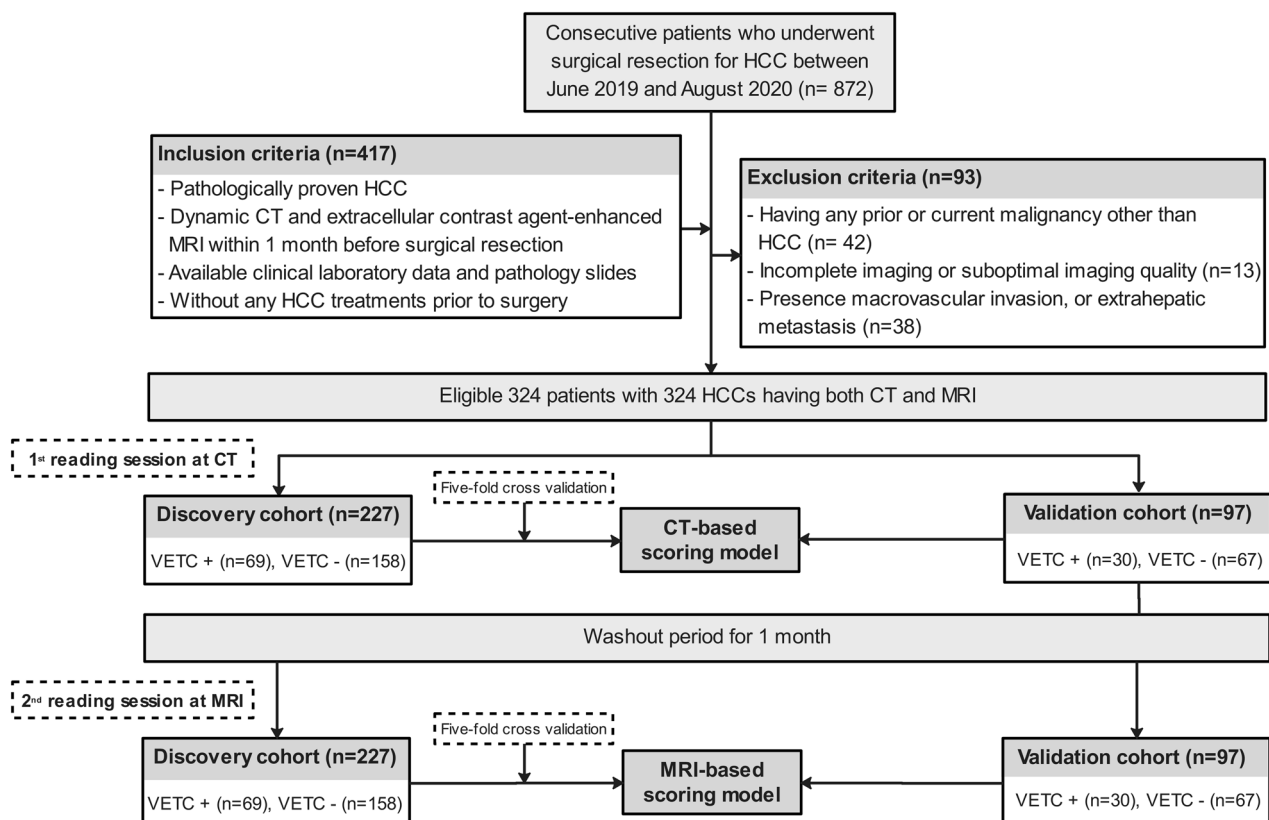


Fig. 1 Study flow diagram. VETC, vessels encapsulating tumor clusters; HCC, hepatocellular carcinoma

Table 1 Clinical and pathological characteristics of patients with hepatocellular carcinoma in the discovery and validation cohorts

Characteristics	Discovery cohort (n = 227)	Validation cohort (n = 97)	p-value
Clinical characteristics			
Age (years) ^a	58.4 (24–85)	59.2 (29–75)	0.384
Gender			0.601
Male	182 (80.2)	80 (82.5)	
Female	45 (19.8)	17 (17.5)	
Cause of liver disease			
Hepatitis B virus	182 (80.2)	72 (72.4)	0.233
Hepatitis C virus	5 (2.2)	1 (1.0)	0.673
Alcohol	18 (7.9)	7 (7.2)	0.826
Nonalcoholic fatty liver disease	5 (2.2)	3 (3.1)	0.700
Others	17 (7.5)	14 (14.4)	0.052
Cirrhosis			0.920
Presence	125 (55.1)	54 (55.7)	
Absent	102 (44.9)	43 (44.3)	
Child-Pugh class			0.256
A	203 (89.4)	88 (90.7)	
B	24 (10.6)	9 (9.3)	
Albumin-bilirubin grade			0.201
1	139 (61.2)	52 (53.6)	
2 or 3	88 (38.8)	45 (46.4)	
Aspartate aminotransferase (U/L)			0.319
≤ 40	126 (55.5)	48 (49.5)	
> 40	101 (44.5)	49 (50.5)	
Alpha-fetoprotein (ng/mL)			0.806
≤ 400	40 (17.6)	16 (16.5)	
> 400	187 (82.4)	81 (83.5)	
Pathological characteristics			
Surgical tumor size (cm) ^a	4.0 (0.8–17.5)	4.2 (1.0–12.5)	0.150
≤ 5.0 cm	161 (70.9)	70 (72.2)	0.821
Edmondson grade			0.863
I or II	124 (54.6)	54 (55.7)	
III or IV	103 (45.4)	43 (44.3)	
Microvascular invasion			0.176
Presence	78 (34.4)	41 (42.3)	
Absent	149 (65.6)	56 (57.7)	
VETC pattern			0.092
Presence	69 (30.4)	30 (30.9)	
Absent	158 (69.6)	67 (69.1)	

Table 1 continued

Characteristics	Discovery cohort (n = 227)	Validation cohort (n = 97)	p-value
Satellite nodule			0.831
Presence	27 (11.9)	15 (15.5)	
Absent	200 (88.1)	82 (84.5)	

LI-RADS Liver Imaging Reporting and Data System, VETC vessels encapsulating tumor clusters
 Unless indicated otherwise, data are numbers of patients, with percentages in parentheses
^aData are medians, with ranges in parentheses

Imaging features and LI-RADS categories of VETC-positive HCC

On both CT and MRI (Table 2), VETC-positive HCCs exhibited a higher frequency of size > 5.0 cm, necrosis or severe ischemia, non-smooth tumor margin, targetoid appearance, intratumor artery, and types of enhancement pattern 3 or 4 compared to VETC-negative HCCs (all $p < 0.05$). Moreover, the tumor-to-liver AP ratio was significantly higher for VETC-positive HCCs on CT ($p = 0.007$), while the tumor-to-liver apparent diffusion coefficient ratio was notably lower for VETC-positive cases on MRI ($p = 0.004$). The LI-RADS algorithm can be applied to evaluate 201 (88.5%) patients who are at high risk for HCC. The proportion of LR-M was significantly higher in VETC-positive HCCs than in VETC-negative HCCs on both CT and MRI (all $p < 0.001$).

Comparison of imaging features and LI-RADS categories between CT and MRI

Table S5 showed that enhancing “capsule”, corona enhancement, mosaic architecture, blood products in mass, and incomplete “capsule” appearance were more frequently observed on MRI compared to CT (all $p < 0.05$). Conversely, the presence of intratumor artery was more commonly found on CT than on MRI ($p = 0.020$). Additionally, the tumor-to-liver AP ratio on MRI was significantly higher than that on CT ($p = 0.008$). Moreover, there were no significant differences in the LI-RADS category distributions of CT and MRI (all $p \geq 0.05$).

Inter-reader and inter-modality agreement of imaging features and LI-RADS categories

Inter-reader and inter-modality agreement of imaging features and LI-RADS categories were presented in Table S6. The inter-reader agreement for imaging features ranged from moderate to almost perfect (κ range: 0.56–0.85) on CT and fair to almost perfect (κ range:

Table 2 Comparison of imaging features and LI-RADS categories between VETC-positive and VETC-negative hepatocellular carcinoma using CT and MRI

Characteristics	CT			MRI		
	VETC (+) (n = 69)	VETC (-) (n = 158)	p-value	VETC (+) (n = 69)	VETC (-) (n = 158)	p-value
Imaging features						
Size > 5.0 cm	32 (46.4)	27 (17.1)	< 0.001	33 (47.8)	32 (20.3)	< 0.001
Nonrim APHE	59 (85.5)	130 (82.3)	0.549	46 (66.7)	130 (82.3)	0.010
Non-peripheral washout	68 (98.6)	155 (98.1)	0.813	68 (98.6)	152 (96.2)	0.456
Enhancing "capsule"	19 (27.5)	36 (22.8)	0.442	52 (75.3)	98 (62.0)	0.051
Corona enhancement	21 (30.4)	31 (19.6)	0.075	31 (44.9)	44 (27.8)	0.012
Fat in mass more than adjacent liver	6 (8.7)	21 (13.3)	0.325	33 (47.8)	78 (49.4)	0.831
Blood products in mass	9 (13.0)	10 (6.3)	0.093	19 (27.5)	17 (10.8)	0.001
Mild-moderate T2 hyperintensity	67 (97.1)	152 (96.2)	0.735
Mosaic architecture	9 (13.0)	9 (5.7)	0.067	21 (30.4)	25 (15.8)	0.012
Restricted diffusion	68 (98.6)	157 (99.4)	0.545
Necrosis or severe ischemia	49 (71.0)	56 (35.4)	< 0.001	52 (75.4)	51 (32.3)	< 0.001
Marked diffusion restriction	46 (66.7)	45 (28.5)	< 0.001
Targetoid appearance	17 (24.6)	13 (8.2)	0.001	20 (29.0)	16 (10.1)	< 0.001
Rim APHE	16 (23.2)	13 (8.2)		17 (24.6)	16 (10.1)	
Delayed central enhancement	2 (2.9)	0 (0.0)		5 (7.2)	1 (0.6)	
Targetoid restriction		10 (14.5)	11 (7.0)	
Intratumor artery	42 (60.9)	22 (13.9)	< 0.001	25 (36.2)	18 (11.4)	< 0.001
Non-smooth tumor margin	49 (71.0)	72 (45.6)	< 0.001	52 (75.4)	54 (34.2)	< 0.001
Incomplete "capsule"	23 (33.3)	35 (22.2)	0.076	54 (78.2)	44 (27.8)	< 0.001
Types of enhancement pattern			< 0.001			< 0.001
1 or 2	36 (52.2)	137 (86.7)		36 (52.2)	130 (82.3)	
3 or 4	33 (47.8)	21 (13.3)		33 (47.8)	28 (17.7)	
Tumor-to-liver AP ratio ^a	1.4 (0.1–3.1)	1.3 (0.1–4.5)	0.007	1.6 (0.1–3.9)	1.5 (0.1–4.0)	0.603
Tumor-to-liver PVP ratio ^a	0.8 (0.3–1.3)	0.7 (0.1–1.3)	0.635	0.8 (0.1–1.5)	0.8 (0.1–2.9)	0.559
Tumor-to-liver ADC ratio ^a	0.9 (0.5–2.2)	1.0 (0.4–2.6)	0.004
LI-RADS category^b	(n = 63)	(n = 138)		(n = 63)	(n = 138)	
LR-M	17 (27.0)	9 (6.5)	< 0.001	20 (31.7)	12 (8.7)	< 0.001
LR-4	1 (1.6)	12 (8.7)	0.067	2 (3.2)	15 (10.9)	0.099
LR-5	45 (71.4)	117 (84.8)	0.027	41 (65.1)	111 (80.4)	0.019

VETC vessels encapsulating tumor clusters, APHE arterial phase hyperenhancement, LI-RADS Liver Imaging Reporting and Data System, PVP portal venous phase, ADC apparent diffusion coefficient

Unless indicated otherwise, data are numbers of patients, with percentages in parentheses.

^a Data are medians, with ranges in parentheses

^b LI-RADS categorization was only applied to patients at high risk for hepatocellular carcinoma (i.e., cirrhosis, chronic hepatitis B viral infection, or current or prior hepatocellular carcinoma)

0.37–0.85) on MRI. For inter-modality agreement, the agreement between CT and MRI on imaging features ranged from slight to almost excellent (κ range: 0.05–0.91). The highest inter-modality agreement was observed for lesion size > 5.0 cm, while the identification of fat in mass more than adjacent liver showed the lowest inter-modality agreement. Regarding LI-RADS categories, both inter-reader and inter-modality agreement demonstrated the highest level of concordance for LR-5 (κ range: 0.65–0.84), followed by LR-M (κ range: 0.59–0.80) and LR-4 (κ range: 0.35–0.73).

Development of CT- and MRI-based models for identifying VETC-positive HCC

Based on the preoperative clinical characteristics and CT features, logistic regression analysis identified five independent predictors of VETC-positive HCC: AFP > 400 ng/mL (odd ratio (OR), 7.31; $p < 0.001$; 10 points), lesion size > 5.0 cm (OR, 3.81; $p = 0.002$; 7 points), intra-tumor artery (OR, 6.07; $p < 0.001$; 9 points), types of enhancement pattern 3 or 4 (OR, 3.74; $p = 0.002$; 7 points), and tumor-to-liver AP ratio > 1.2 (OR, 4.86; $p = 0.001$; 8 points) (Table 3). Similarly, among preoperative clinical

Table 3 Logistic regression analysis for CT-based identification of VETC-positive hepatocellular carcinoma in the discovery cohort

Variable	Univariate analysis		Multivariate analysis			
	Odds ratio	p-value	Odds ratio	p-value	Regression coefficient	Score assigned
Preoperative clinical characteristics						
Alpha-fetoprotein > 400 ng/mL	5.37 (2.64, 10.92)	< 0.001	7.31 (2.69, 19.84)	< 0.001	1.99	10/0
Aspartate aminotransferase > 40 U/L	0.87 (0.49, 1.53)	0.622
Child-Pugh class B	1.16 (0.47, 2.86)	0.741
Albumin-bilirubin grade 2 or 3	0.86 (0.48, 1.54)	0.605
Preoperative CT features						
Size > 5.0 cm	4.20 (2.24, 7.87)	< 0.001	3.81 (1.66, 8.75)	0.002	1.34	7/0
Corona enhancement	1.79 (0.94, 3.42)	0.077
Mosaic architecture	3.67 (1.00, 13.44)	0.050
Blood products in mass	2.22 (0.86, 5.74)	0.100
Necrosis or severe ischemia	4.46 (2.42, 8.24)	< 0.001	1.50 (0.61, 3.70)	0.375	0.41	...
Intratumor artery	9.62 (4.97, 18.62)	< 0.001	6.07 (2.72, 13.54)	< 0.001	1.80	9/0
Incomplete "capsule"	1.76 (0.94, 3.29)	0.077
Non-smooth tumor margin	2.93 (1.59, 5.37)	0.001	1.79 (0.87, 4.13)	0.169	0.58	...
Types of enhancement patterns 3 or 4	5.98 (3.09, 11.56)	< 0.001	3.74 (1.60, 8.71)	0.002	1.32	7/0
Tumor-to-liver AP ratio > 1.2	4.94 (2.36, 10.35)	< 0.001	4.86 (1.95, 12.15)	0.001	1.58	8/0
Tumor-to-liver PVP ratio ≤ 0.5	3.37 (0.97, 11.71)	0.056

VETC vessels encapsulating tumor clusters, AP arterial phase, PVP portal venous phase
Data in parentheses are 95% CI

Table 4 Logistic regression analysis for MRI-based identification of VETC-positive hepatocellular carcinoma in the discovery cohort

Variable	Univariate analysis		Multivariate analysis			
	Odds ratio	p-value	Odds ratio	p-value	Regression coefficient	Score assigned
Preoperative clinical characteristics						
Alpha-fetoprotein > 400 ng/mL	5.37 (2.64, 10.92)	< 0.001	5.21 (1.94, 14.01)	0.001	1.65	7/0
Aspartate aminotransferase > 40 U/L	0.87 (0.49, 1.53)	0.622
Child-Pugh class B	1.16 (0.47, 2.86)	0.741
Albumin-bilirubin grade 2 or 3	0.86 (0.48, 1.54)	0.605
Preoperative MRI features						
Size > 5.0 cm	3.61 (1.96, 6.65)	< 0.001	1.39 (0.48, 4.02)	0.548	0.32	...
Corona enhancement	2.21 (1.17, 3.81)	0.031	1.38 (0.51, 3.72)	0.525	0.32	...
Mosaic architecture	2.33 (1.19, 4.54)	0.013	0.66 (0.21, 2.09)	0.476	0.42	...
Blood products in mass	3.15 (1.52, 6.54)	0.002	0.42 (0.13, 1.40)	0.156	0.87	...
Necrosis or severe ischemia	6.42 (3.38, 12.19)	< 0.001	7.78 (2.92, 20.75)	< 0.001	2.05	9/0
Intratumor artery	4.42 (2.21, 8.85)	< 0.001	2.80 (1.00, 7.83)	0.050	1.03	...
Incomplete "capsule"	9.33 (4.78, 18.22)	< 0.001	10.10 (3.93, 25.95)	< 0.001	2.31	10/0
Non-smooth tumor margin	5.89 (3.11, 11.16)	< 0.001	7.13 (2.86, 17.80)	< 0.001	1.96	8/0
Marked diffusion restriction	5.02 (2.73, 9.23)	< 0.001	7.74 (2.99, 20.01)	< 0.001	2.05	9/0
Types of enhancement patterns 3 or 4	4.26 (2.28, 7.95)	< 0.001	1.70 (0.66, 4.35)	0.268	0.53	...
Tumor-to-liver AP ratio > 1.6	2.12 (1.20, 3.77)	0.010	1.91 (0.81, 4.54)	0.141	0.65	...
Tumor-to-liver PVP ratio ≤ 0.5	1.58 (0.86, 2.91)	0.141
Tumor-to-liver ADC ratio ≤ 0.9	2.72 (1.50, 4.91)	0.001	1.08 (0.42, 2.78)	0.868	0.80	...

VETC vessels encapsulating tumor clusters, AP arterial phase, PVP portal venous phase, ADC
Data in parentheses are 95% CI




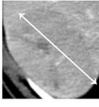

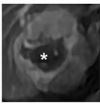

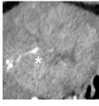

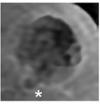

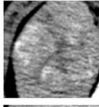

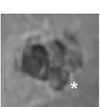



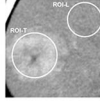

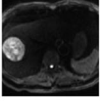
a CT-based scoring model				b MRI-based scoring model			
Predictors	Definitions	Schematics	Examples	Predictors	Definitions	Schematics	Examples
Serum alpha-fetoprotein ≤ 400 ng/ml / > 400 ng/mL 0 / 10 points				Serum alpha-fetoprotein ≤ 400 ng/ml / > 400 ng/mL 0 / 7 points			
Tumor size > 5.0 cm Absent / Present 0 / 7 points	Presence of discrete arterial enhancement within the tumor.			Necrosis or severe ischemia Absent / Present 0 / 9 points	Presence of unequivocal intralesional necrosis or severe ischemia.		
Intratumor artery Absent / Present 0 / 9 points	Largest outer-edge-to-outer-edge dimension of an observation > 5.0 cm.			Incomplete "capsule" Absent / Present 0 / 10 points	An absence of "capsule" or presence of disrupted "capsule" in any imaging plane.		
Types of enhancement pattern 3 or 4 Absent / Present 0 / 7 points	Type-3: Heterogeneous enhancement with septations during arterial and portal venous phases.			Nonsmooth tumor margin Absent / Present 0 / 8 points	The outer contour of a mass at least in part, irregular or has areas of bulging, nodular projection, or infiltration.		
	Type-4: Heterogeneous enhancement with irregular ring-like structures during arterial and portal venous phases.						
Tumor-to-liver ratio at arterial phase ≤ 1.2 / > 1.2 0 / 8 points	The ratios of tumor-to-liver attenuation on arterial phase.			Marked diffusion restriction Absent / Present 0 / 9 points	Intensity is similar to or higher than nonironoverloaded spleen, not caused only by T2 shine-through at MRI.		

Fig. 2 Graphical illustration of the CT model and MRI model. **a** Lesions with scores > 17 points were classified as vessels encapsulating tumor clusters (VETC)-positive hepatocellular carcinoma (HCC) using the CT model, **(b)** whereas lesions with scores > 21 points were classified as VETC-positive HCC using the MRI model

characteristics and MRI features, AFP > 400 ng/mL (OR, 5.21; $p = 0.001$; 7 points), necrosis or severe ischemia (OR, 7.78; $p < 0.001$; 9 points), incomplete "capsule" (OR, 10.10; $p < 0.001$; 10 points), non-smooth tumor margin (OR, 7.13; $p < 0.001$; 8 points), and marked diffusion restriction (OR, 7.74; $p < 0.001$; 9 points) were found to be independent predictors of VETC-positive HCCs (Table 4). Subsequently, a CT-based scoring model and an MRI-based scoring model were subsequently constructed, with cutoff values of > 17 points and > 21 points, respectively (Fig. 2).

Comparison of diagnostic performance between CT- and MRI-based models

Performances of the developed models for identifying VETC-positive HCC are presented in Table 5, and Fig. 3. In the validation cohort, the CT-based model demonstrated a sensitivity of 76.7% and the MRI-based model showed a sensitivity of 86.7%, with no statistically significant difference ($p = 0.375$). Regarding specificity, the CT-based model achieved 83.6% while the MRI-based model achieved 74.6%, also without statistical significance ($p = 0.180$). Both models showed comparable AUCs for identifying VETC-positive HCCs in the discovery cohort

(0.82 vs. 0.85, $p = 0.490$) and validation cohort (0.80 vs. 0.81, $p = 0.910$) (Fig. 4a, b). Calibration curves confirmed a strong agreement between the predicted probability of VETC by the models and surgically-proven VETC in both cohorts (Fig. 4c, d).

In subgroup analyses of HCC cases with sizes ≤ 5.0 cm and ≤ 3.0 cm, the comparative results of CT- and MRI-based scoring models were consistent with the overall cohorts (Fig. S1). No significant differences were observed in terms of sensitivity, specificity, and AUC between the two scoring models in the validation cohorts (all $p \geq 0.05$).

Discussion

In the current study, we constructed and validated CT- and MRI-based scoring models for the identification of VETC-positive HCCs. Our results indicated that the CT-based model displayed similar performance to the MRI-based model when using pathological results as the reference standard. Compared to the previous studies [7, 12, 14, 16], our research extensively evaluated potential predictors, including clinical characteristics, traditional qualitative and quantitative imaging features. This thorough evaluation may enhance the accuracy of the

Table 5 Comparison of performance between CT and MRI models for identifying VETC-positive hepatocellular carcinoma

Parameter	Discovery cohort			Validation cohort		
	CT-based scoring model	MRI-based scoring model	<i>p</i> -value	CT-based scoring model	MRI-based scoring model	<i>p</i> -value
Total lesions	(<i>n</i> = 227)			(<i>n</i> = 97)		
AUC	0.82 (0.77, 0.87)	0.85 (0.79, 0.89)	0.490	0.80 (0.71, 0.88)	0.81 (0.71, 0.88)	0.910
Sensitivity (%)	72.5 (60.4, 82.5) (50/69)	87.0 (76.7, 93.9) (60/69)	0.052	76.7 (57.7, 90.1) (23/30)	86.7 (69.3, 96.2) (26/30)	0.375
Specificity (%)	91.9 (86.3, 95.6) (145/158)	82.3 (75.4, 87.9) (130/158)	0.003	83.6 (72.5, 91.5) (56/67)	74.6 (62.5, 84.5) (50/67)	0.180
PPV (%)	79.4 (69.1, 86.9) (50/63)	68.2 (60.2, 75.2) (60/88)	...	67.7 (54.1, 78.8) (23/34)	60.5 (49.8, 70.2) (26/43)	...
NPV (%)	88.4 (83.8, 91.8) (145/164)	93.5 (88.8, 96.4) (130/139)	...	88.9 (72.3, 88.6) (56/63)	92.6 (83.2, 96.9) (50/54)	...
Lesions ≤ 5.0 cm	(<i>n</i> = 161)			(<i>n</i> = 70)		
AUC	0.77 (0.70, 0.84)	0.87 (0.80, 0.92)	0.060	0.69 (0.57, 0.80)	0.77 (0.60, 0.86)	0.347
Sensitivity (%)	60.0 (42.1, 76.1) (21/35)	88.6 (73.5, 96.8) (31/35)	0.013	53.3 (26.6, 78.7) (8/15)	73.3 (44.9, 92.2) (11/15)	0.375
Specificity (%)	94.4 (88.9, 97.7) (119/126)	84.9 (77.5, 90.7) (107/116)	0.004	85.5 (73.3, 93.5) (47/55)	80.0 (67.0, 89.6) (44/55)	0.508
PPV (%)	75.0 (58.2, 86.6) (21/28)	62.0 (51.5, 71.5) (31/50)	...	50.0 (31.1, 68.9) (8/16)	50.0 (35.2, 64.8) (11/22)	...
NPV (%)	89.5 (85.0, 92.7) (119/133)	96.4 (91.4, 98.5) (107/111)	...	87.0 (79.5, 92.1) (47/54)	91.7 (82.5, 96.3) (44/48)	...
Lesions ≤ 3.0 cm	(<i>n</i> = 105)			(<i>n</i> = 41)		
AUC	0.71 (0.60, 0.83)	0.83 (0.73, 0.93)	0.091	0.74 (0.55, 0.92)	0.85 (0.69, 1.00)	0.140
Sensitivity (%)	47.4 (24.5, 71.1) (9/19)	78.9 (54.4, 93.9) (15/19)	0.070	50.0 (15.7, 84.3) (4/8)	75.0 (34.9, 96.8) (6/8)	0.500
Specificity (%)	95.3 (88.5, 98.7) (82/86)	87.2 (78.3, 93.4) (75/86)	0.065	97.0 (84.2, 99.9) (32/33)	97.0 (84.2, 99.9) (32/33)	1.000
PPV (%)	69.2 (43.6, 86.7) (9/13)	57.7 (42.8, 71.3) (15/26)	...	80.0 (34.0, 96.9) (4/5)	85.7 (45.5, 97.7) (6/7)	...
NPV (%)	89.1 (84.2, 92.6) (82/92)	94.9 (88.7, 97.8) (75/79)	...	88.9 (80.0, 94.1) (32/36)	94.1 (82.2, 98.2) (32/34)	...

VETC vessels encapsulating tumor clusters, AUC area under the receiver operating curve, PPV positive predictive value, NPV negative predictive value
Data in parentheses are 95% CIs, and data in brackets are numbers of patients

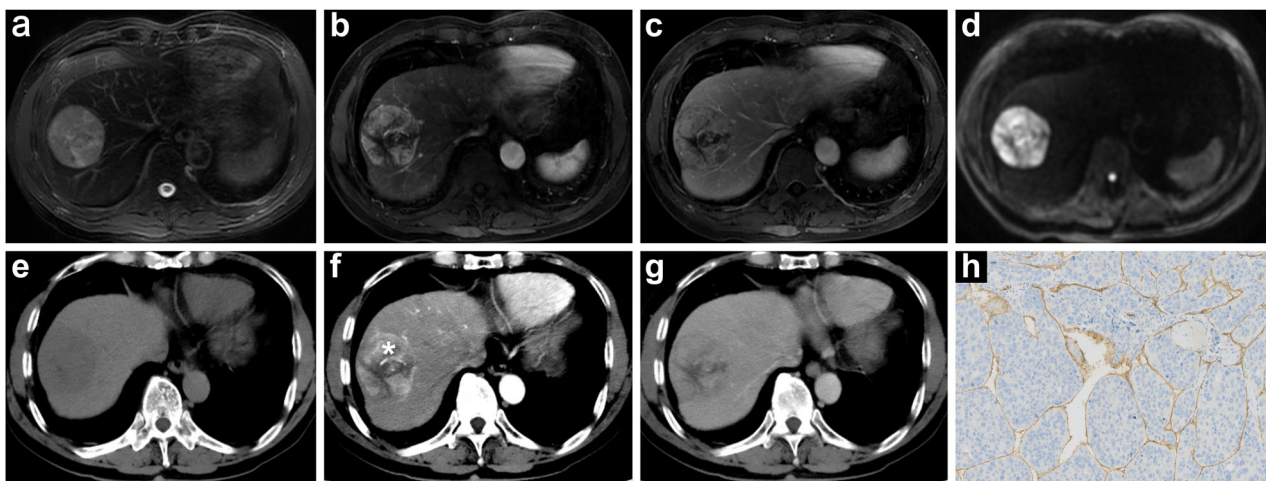


Fig. 3 A 64-year-old man with chronic hepatitis B infection and vessels encapsulating tumor clusters (VETC)-positive hepatocellular carcinoma (HCC) using (a–d) MRI and (e–g) CT. Both CT and MRI models classified the lesion as VETC-positive HCC. The patient’s preoperative serum alpha-fetoprotein level was 487.8 ng/mL. MRI revealed heterogeneous enhancement with septations on (a) T2-weighted image, (b) arterial phase, and (c) portal venous phase, along with marked diffusion restriction on (d) diffusion-weighted image within the lesion. CT demonstrated a tumor size of 5.7 cm, with the presence of an intratumoral artery (star) and heterogeneous enhancement with septations on the (f) arterial phase and (g) portal venous phase. h CD34 immunostaining confirmed the presence of the VETC pattern, validating the prediction made by the models

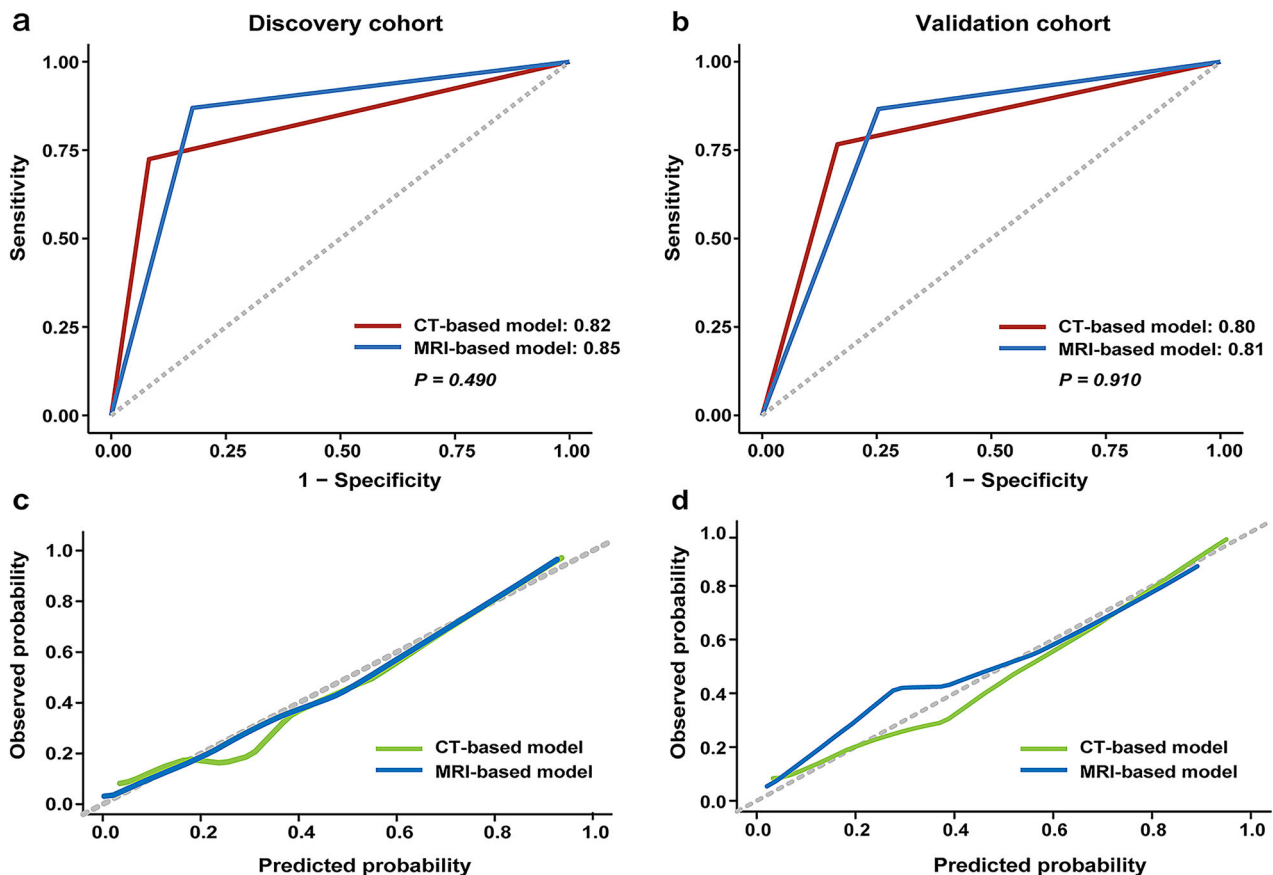


Fig. 4 Performances of the CT model and MRI model in identifying vessels encapsulating tumor clusters (VETC)-positive hepatocellular carcinoma (HCC). In both the (a) discovery and (b) valid cohorts, receiver operating characteristic curve analyses showed that the CT model and MRI model exhibited comparable areas under the curves. In both the (c) discovery and (d) validation cohorts, the calibration curves of the CT model and the MRI model displayed good agreement

developed models and enable more reliable prediction of VETC-positive HCCs.

The variations in integrated imaging predictors within CT- and MRI-based models may be attributed to the differential capabilities of these modalities in detecting specific features. Specifically, MRI exhibited a higher rate of identifying the incomplete tumor “capsule” appearance compared to CT, independently predicting VETC-positive HCCs. This improved detection on MRI is likely due to its superior contrast resolution and detailed tumor assessment ability [10]. Recent comparative analysis has also shown that extracellular agent-enhanced MRI exhibited significantly higher sensitivity in detecting tumor capsules than contrast-enhanced CT [24]. Additionally, dilated vasculature, considered a biomarker for angiogenesis in HCC, has been reported to correlate with the VETC pattern [13]. Similar to previous findings, our study showed that the presence of the intratumor artery was an independent predictor of the VETC pattern in the CT-

based model rather than the MRI-based model. On the other hand, MRI offers additional imaging sequences apart from CT, such as T2-weighted and diffusion-weighted imaging. Our results identified the presence of marked diffusion restriction as an independent predictor of VETC-positive HCCs using MRI. Diffusion-weighted imaging provides insights into increased cell proliferation in more aggressive HCCs, offering valuable information beyond tumor angiogenesis [11, 25]. Thus, the utilization of multiparametric MRI may enhance the diagnostic sensitivity of the MRI-based model and aid in evaluating the VETC pattern. Consistently, our results showed a tendency towards higher diagnostic sensitivity in the MRI-based model compared to the CT-based model; however, no significant difference was found between the two models in the validation cohort. One plausible explanation for this result might be the low frequency of VETC-positive cases and limited sample size, which could affect the statistical power of the results [26]. Further

research with a larger population is necessary to validate our findings.

Based on our results, serum AFP > 400 ng/mL emerged as the sole clinical predictor incorporated in both the CT-based and MRI-based models. As a robust biomarker of HCC, elevated serum AFP levels have shown associations with poor tumor differentiation [27] and unfavorable clinical prognosis [28, 29]. Prior research has also indicated that serum AFP > 400 ng/mL can serve as an independent predictive factor for the presence of VETC or microvascular invasion in HCC [30]. Furthermore, it is noteworthy that the limited inclusion of clinical indicators in the developed models may underscore the crucial role of imaging procedures in the non-invasive assessment of VETC patterns.

In terms of inter-modality agreement, our study revealed a wide range of κ values when assessing imaging features. There was a high level of agreement observed (κ : 0.91) regarding lesion size > 5.0 cm. Conversely, the presence of fat in mass more than in adjacent liver showed the lowest inter-modality agreement (κ : 0.05), which can be attributed to the utilization of chemical shift imaging in MRI, known for its accuracy in quantifying intratumoral fat [31]. As a result, MRI exhibited a significantly higher detection rate of fat in mass more than adjacent liver when compared to CT (48.9% vs. 11.9%, $p < 0.001$).

In our study, VETC-positive HCCs were more frequently assigned to LR-M than VETC-negative cases, with rim APHE being the predominant LR-M characteristic identified on both CT and MRI. One possible explanation for the rim APHE is the abundance of fibrotic stroma in tumors, which may hinder global enhancement of the HCC [32]. Additionally, central necrosis or severe ischemia in rapidly growing HCC may also contribute to the occurrence of rim APHE [32–34]. Importantly, our study utilized both CT and MRI modalities to evaluate the LI-RADS categories of VETC-positive HCCs. This analysis not only verified but also expanded upon the findings of a prior study that solely assessed rim APHE on CT [12].

The present study had several limitations. First, this was a single-center retrospective study. Although our scoring models underwent five-fold cross-validation and verification in an independent cohort, the lack of formal external validation should be acknowledged. Second, the limited number of VETC-positive HCC cases in the validation cohort may potentially impede the robustness and generalizability of the findings. Third, the inclusion of HCC patients who underwent both preoperative CT and MRI, with the evaluation of imaging features conducted in the order of CT followed by MRI, could introduce potential bias. Finally, the scoring models developed in this study

were based on traditional quantitative and qualitative imaging features. Future research should focus on comparing the diagnostic capabilities of radiomics models based on CT and MRI for VETC-positive HCCs.

In conclusion, the present study successfully developed and validated practical scoring modes for the preoperative identification of VETC-positive HCCs using dynamic CT and MRI with extracellular contrast agent, respectively. Our findings suggested that both CT- and MRI-based models demonstrated comparable performance for predicting VETC-positive HCCs. Further multicenter prospective studies are warranted to refine the developed models and verify the findings obtained in this study.

Abbreviations

AFP	Alpha-fetoprotein
APHE	Arterial phase hyperenhancement
AUC	Area under the curve
CT	Computed tomography
HCC	Hepatocellular carcinoma
LI-RADS	Liver Imaging Reporting and Data System
MRI	Magnetic resonance imaging
OR	Odds ratio
ROC	Receiver operating characteristic
VETC	Vessels encapsulating tumor clusters

Supplementary information

The online version contains supplementary material available at <https://doi.org/10.1007/s00330-024-10944-9>.

Funding

This study has received funding from the Zhejiang Provincial Natural Science Foundation Committee-Zhejiang Society for Mathematical Medicine Joint Fund Major Project (LSD19H180003) and the National Natural Science Foundation of China (12090020 and 12090025).

Compliance with ethical standards

Guarantor

The scientific guarantor of this publication is Feng Chen.

Conflict of interest

The authors of this manuscript declare no relationships with any companies, whose products or services may be related to the subject matter of the article.

Statistics and biometry

Feng Chen has significant statistical expertise.

Informed consent

Written informed consent was waived by the Institutional Review Board.

Ethical approval

Institutional Review Board approval was obtained.

Study subjects or cohorts overlap

None.

Methodology

- Retrospective
- Diagnostic study
- Performed at one institution

Received: 15 February 2024 Revised: 30 April 2024 Accepted: 19 June 2024
Published online: 12 July 2024

References

- Fang JH, Zhou HC, Zhang C et al (2015) A novel vascular pattern promotes metastasis of hepatocellular carcinoma in an epithelial-mesenchymal transition-independent manner. *Hepatology* 62:452–465
- Liu K, Dennis C, Prince DS et al (2023) Vessels that encapsulate tumour clusters vascular pattern in hepatocellular carcinoma. *JHEP Rep* 5:100792
- Renne SL, Woo HY, Allegra S et al (2020) Vessels encapsulating tumor clusters (VETC) is a powerful predictor of aggressive hepatocellular carcinoma. *Hepatology* 71:183–195
- Fang JH, Xu L, Shang LR et al (2019) Vessels that encapsulate tumor clusters (VETC) pattern is a predictor of sorafenib benefit in patients with hepatocellular carcinoma. *Hepatology* 70:824–839
- Kawasaki J, Toshima T, Yoshizumi T et al (2021) Prognostic impact of vessels that encapsulate tumor cluster (VETC) in patients who underwent liver transplantation for hepatocellular carcinoma. *Ann Surg Oncol* 28:8186–8195
- Chen ZY, Guo ZX, Lu LH et al (2021) The predictive value of vessels encapsulating tumor clusters in treatment optimization for recurrent early-stage hepatocellular carcinoma. *Cancer Med* 10:5466–5474
- Meng XP, Tang TY, Zhou Y et al (2023) Predicting post-resection recurrence by integrating imaging-based surrogates of distinct vascular patterns of hepatocellular carcinoma. *JHEP Rep* 5:100806
- Heimbach JK, Kulik LM, Finn RS et al (2018) AASLD guidelines for the treatment of hepatocellular carcinoma. *Hepatology* 67:358–380
- European Association for the Study of the Liver (2018) EASL clinical practice guidelines: management of hepatocellular carcinoma. *J Hepatol* 69:182–236
- Roberts LR, Sirlin CB, Zaiem F et al (2018) Imaging for the diagnosis of hepatocellular carcinoma: a systematic review and meta-analysis. *Hepatology* 67:401–421
- Ronot M, Chernyak V, Burgoyne A et al (2023) Imaging to predict prognosis in hepatocellular carcinoma: current and future perspectives. *Radiology* 307:e221429
- Feng Z, Li H, Zhao H et al (2021) Preoperative CT for characterization of aggressive macrotrabecular-massive subtype and vessels that encapsulate tumor clusters pattern in hepatocellular carcinoma. *Radiology* 300:219–229
- Kitao A, Matsui O, Zhang Y et al (2023) Dynamic CT and gadoxetic acid-enhanced MRI characteristics of P53-mutated hepatocellular carcinoma. *Radiology* 306:e220531
- Fan Y, Yu Y, Hu M et al (2021) Imaging features based on Gd-EOB-DTPA-enhanced MRI for predicting vessels encapsulating tumor clusters (VETC) in patients with hepatocellular carcinoma. *Br J Radiol* 94:20200950
- Chen FM, Du M, Qi X et al (2023) Nomogram estimating vessels encapsulating tumor clusters in hepatocellular carcinoma from preoperative gadoxetate disodium-enhanced MRI. *J Magn Reson Imaging* 57:1893–1905
- Dong X, Yang J, Zhang B et al (2023) Deep learning radiomics model of dynamic contrast-enhanced MRI for evaluating vessels encapsulating tumor clusters and prognosis in hepatocellular carcinoma. *J Magn Reson Imaging*. <https://doi.org/10.1002/jmri.28745>
- Heo S, Kang HJ, Choi SH et al (2023) Proliferative hepatocellular carcinomas in cirrhosis: patient outcomes of LI-RADS category 4/5 and category M. *Eur Radiol*. <https://doi.org/10.1007/s00330-023-10305-y>
- Yang J, Jiang H, Xie K et al (2022) Profiling hepatocellular carcinoma aggressiveness with contrast-enhanced ultrasound and gadoxetate disodium-enhanced MRI: An intra-individual comparative study based on the Liver Imaging Reporting and Data System. *Eur J Radiol* 154:110397
- Choi SH, Lee SS, Park SH et al (2019) LI-RADS classification and prognosis of primary liver cancers at gadoxetic acid-enhanced MRI. *Radiology* 290:388–397
- Bae JS, Lee JM, Yoon JH et al (2021) Evaluation of LI-RADS version 2018 treatment response algorithm for hepatocellular carcinoma in liver transplant candidates: intraindividual comparison between CT and hepatobiliary agent-enhanced MRI. *Radiology* 299:336–345
- Kawamura Y, Ikeda K, Hirakawa M et al (2010) New classification of dynamic computed tomography images predictive of malignant characteristics of hepatocellular carcinoma. *Hepatol Res* 40:1006–1014
- Chen J, Xia C, Duan T et al (2021) Macrotrabecular-massive hepatocellular carcinoma: imaging identification and prediction based on gadoxetic acid-enhanced magnetic resonance imaging. *Eur Radiol* 31:7696–7704
- Moons KG, Altman DG, Reitsma JB et al (2015) Transparent reporting of a multivariable prediction model for individual prognosis or diagnosis (TRIPOD): explanation and elaboration. *Ann Intern Med* 162:W1–73
- Cannella R, Ronot M, Sartoris R et al (2021) Enhancing capsule in hepatocellular carcinoma: intra-individual comparison between CT and MRI with extracellular contrast agent. *Diagn Interv Imaging* 102:735–742
- Jiang H, Wei J, Fu F et al (2022) Predicting microvascular invasion in hepatocellular carcinoma: a dual-institution study on gadoxetate disodium-enhanced MRI. *Liver Int* 42:1158–1172
- Schuurs AH, Wu MK, Wesselink PR, Duivenvoorden HJ (1993) Endodontic leakage studies reconsidered. Part II. Statistical aspects. *Int Endod J* 26:44–52
- Yang T, Wei H, Wu Y et al (2023) Predicting histologic differentiation of solitary hepatocellular carcinoma up to 5 cm on gadoxetate disodium-enhanced MRI. *Insights Imaging* 14:3
- Mehta N, Heimbach J, Harnois DM et al (2017) Validation of a risk estimation of tumor recurrence after transplant (RETREAT) score for hepatocellular carcinoma recurrence after liver transplant. *JAMA Oncol* 3:493–500
- Wei H, Fu F, Jiang H et al (2023) Development and validation of the OSASH score to predict overall survival of hepatocellular carcinoma after surgical resection: a dual-institutional study. *Eur Radiol* 33:7631–7645
- Yang J, Dong X, Wang G et al (2023) Preoperative MRI features for characterization of vessels encapsulating tumor clusters and microvascular invasion in hepatocellular carcinoma. *Abdom Radiol (NY)* 48:554–566
- Faure A, Dioguardi Burgio M, Cannella R et al (2024) Imaging and prognostic characterization of fat-containing hepatocellular carcinoma subtypes. *Radiol Med*. <https://doi.org/10.1007/s11547-024-01807-w>
- Rhee H, An C, Kim HY, Yoo JE, Park YN, Kim MJ (2019) Hepatocellular carcinoma with irregular rim-like arterial phase hyperenhancement: more aggressive pathologic features. *Liver Cancer* 8:24–40
- Choi SY, Kim SH, Park CK et al (2018) Imaging features of gadoxetic acid-enhanced and diffusion-weighted MR imaging for identifying cytokeratin 19-positive hepatocellular carcinoma: a retrospective observational study. *Radiology* 286:897–908
- Rhee H, Cho ES, Nahm JH et al (2021) Gadoxetic acid-enhanced MRI of macrotrabecular-massive hepatocellular carcinoma and its prognostic implications. *J Hepatol* 74:109–121

Publisher's Note

Springer Nature remains neutral with regard to jurisdictional claims in published maps and institutional affiliations.

Springer Nature or its licensor (e.g. a society or other partner) holds exclusive rights to this article under a publishing agreement with the author(s) or other rightsholder(s); author self-archiving of the accepted manuscript version of this article is solely governed by the terms of such publishing agreement and applicable law.